Steel and Composite Structures, *Vol. 36, No. 1 (2020) 103-118*
DOI: https://doi.org/10.12989/scs.2020.36.1.103

Experimental and numerical study on static behavior of grouped large-headed studs embedded in UHPC

Yuqing Hu[1], Guotang Zhao[2], Zhiqi He[1], Jianan Qi[1] and Jingquan Wang[*1]

[1]*Key Laboratory of Concrete and Prestressed Concrete Structures of Ministry of Education, Southeast University, Nanjing 210096, China*
[2]*China State Railway Group Co., Ltd. Beijing 100844, China*

(*Received March 9, 2019, Revised June 11, 2020, Accepted June 27, 2020*)

Abstract. The static behavior of grouped large-headed studs (d = 30 mm) embedded in ultra-high performance concrete (UHPC) was investigated by conducting push-out tests and numerical analysis. In the push-out test, no splitting cracks were found in the UHPC slab, and the shank failure control the shear capacity, indicating the large-headed stud matches well with the mechanical properties of UHPC. Besides, it is found that the shear resistance of the stud embedded in UHPC is 11.4% higher than that embedded in normal strength concrete, indicating that the shear resistance was improved. Regarding the numerical analysis, the parametric study was conducted to investigate the influence of the concrete strength, aspect ratio of stud, stud diameter, and the spacing of stud in the direction of shear force on the shear performance of the large-headed stud. It is found that the stud diameter and stud spacing have an obvious influence on the shear resistance. Based on the test and numerical analysis results, a formula was established to predict the load-slip relationship. The comparison indicates that the predicted results agree well with the test results. To accurately predict the shear resistance of the stud embedded in UHPC, a design equation for shear strength is proposed. The ratio of the calculation results to the test results is 0.99.

Keywords: grouped large-headed stud; UHPC slab; UHPC shear pocket; push-out test; numerical analysis; static behavior

1. Introduction

Headed studs are widely used in steel-composite structures as the shear connector. It not only connects the concrete slab with steel beam but also transfers the shear force at the interlayer between the steel and concrete. Previous research indicated that the mechanical behavior and shear strength of headed stud affected by many factors, especially the compressive strength and elastic modulus (Viest 1956, Ollgaard *et al.* 1971, Oehlers 1992, Oehlers 1995, Bezerra *et al.* 2018). In the high-stress area of the composite bridge, numerous studs, withing the small diameter, were arranged to resist the shear stress, resulting in a mass of welding work. Previous researches have indicated that using studs with larger diameter can mitigate these problems (An *et al.* 1996, Badie *et al.* 2002, Shim *et al.* 2004, Lee *et al.* 2005). However, it should be noted that the transverse splitting force in concrete slab increases with the increase of stud diameter. Thus, it is unreasonable to use the large-headed stud in the steel-concrete composite structures, attributing the reason that the splitting cracks are easy to form in normal concrete slab.

Ultra-high-performance concrete (UHPC) as a composite material, which offers significant superior mechanical properties, such as compressive and tensile strength, as well as excellent durability compared with conventional concrete (An *et al.* 2019a, An *et al.* 2019b), has been introduced to steel-concrete composite structures to achieve much stronger and more compact shear connection (Hamoda *et al.* 2017, Kang *et al.* 2014, Le *et al.* 2018). It provides an opportunity for the application of large-headed stud in steel-concrete composite structure.

Previous research has reported that the failure modes of steel-UHPC composite structures is different from that of the normal steel-concrete composite structures, the shear capacity shank is usually controlled by the shank failure of the stud without concrete crushing (Kim *et al.* 2015, Kruszewski *et al.* 2018). Besides, it is found that the shear capacity of the former is improved when the headed stud is embedded in UHPC (Wang *et al.* 2019, Wang *et al.* 2018).

Currently, the shear behavior of headed stud shear connectors embedded in the UHPC deck has been investigated. The static and fatigue behavior of short-headed studs embedded in UHPC was investigated by Cao *et al.* (2017). Their research results indicated that current design codes underestimated the shear strength of the headed studs. Kim *et al.* (2015) investigated the static behavior of the headed stud with a diameter of 16 mm and 22 mm. Test results showed that no splitting crack was found in the UHPC slab when the aspect ratio reduced from 4 to 3.1. The effect of the spacing of stud on the static behavior of stud, of which diameter is 13 mm and 22 mm, was studied by Luo *et al.* (2015). It was found that grouped studs arranged densely, with a pitch length of only 3.5d, can still possess shear strength (per stud) not less than 90% of the shear strength of a single stud. The effect of the shank diameter and aspect ratio on failure modes, initial stiffness,

*Corresponding author, Professor
E-mail: wangjingquan@seu.edu.cn

http://www.techno-press.org/?journal=scs&subpage=8
ISSN: 1229-9367 (Print), 1598-6233 (Online)

Table 1 Mix proportions of UHPC and NSC

Component	Weight	
	UHPC (kg/m^3)	NSC (kg/m^3)
Cement	732	285
Broken Stone 5-8 mm	397	1003
Sand 0-5 mm	737	757
Silica fume	85	-
High active admixture	299	195
Steel fiber type I	80	-
Steel fiber type II	80	-
Water	165	158
Superplasticizer	22.7	4
Water-binder ratio (W/B)	0.16	0.33

Note: Steel fiber type I denotes straight steel fibers with D = 0.2 mm and L = 13 mm; Steel fiber type II denotes end-hooked steel fibers with D = 0.2 mm and L = 13 mm, where D denotes fiber diameter and L denotes fiber length

Table 2 Mechanical properties of concrete

Material	Cubic compressive strength f_c (MPa)	Direct tensile strength f_t (MPa)	Young's modulus E_c (GPa)
NC	49	4.1	35
UHPC	124	6.7	48

ultimate strength, and ductility were investigated by Wang *et al*. (2017) via push-out tests. His study indicated that the ductility of headed stud embedded in the UHPC slab was less than the requirements in Eurocode 4. The static behavior of single large stud in steel-UHPC composite structures was investigated by Wang *et al.* (2019), the experimental results showed that no splitting cracks were found for the UHPC slab with studs of 30 mm diameter.

To promote the use of the large-headed stud in steel-UHPC composite structures, the static behavior of grouped large-headed studs (d > 25 mm) embedded in the UHPC slab and UHPC shear pocket, especially the effect of the arrangement of the large-headed studs on their shear performance should be studied. Moreover, it should be noted that current design codes are usually used to predict the shear capacity of stud, which are established based on the steel-concrete composite structures. The strength of UHPC is far greater than that of normal strength concrete, and the excellent mechanical properties of UHPC is beneficial for improving the shear capacity of stud due to the interaction between stud and UHPC, resulting in the underestimation using the shear strength formula in these design codes.

In this study, the static behavior of grouped large-headed stud embedded in UHPC slab and UHPC shear pocket, including shear strength, shear load-slip curve, and shear stiffness was obtained was investigated through the push-out test and systematic numerical analysis. The influence of concrete strength, the aspect ratio of stud, stud diameter, and spacing of stud in the direction of shear force on the static behavior of grouped headed stud was investigated through a parametric study. Based on the test results in this paper and previous research, the expression of load-slip relationship and calculations formula of shear strength were proposed with consideration of characteristics of steel-UHPC composite structures

2. Experimental investigation and results

2.1 UHPC mixture and properties

The mixture proportion of ultrahigh-performance concrete (UHPC) and normal strength concrete (NSC) was shown in Table 1. The density and specific surface area of cement are 3170 kg/m^3 and 388 m^2/kg, respectively, and the density and specific surface area of silica are 21.4 m^2/g and 185 kg/m^3, respectively. Coarse aggregate of broken stone distributed from 5 mm to 8 mm and river sand was used in UHPC, aiming at reducing autogenous shrinkage and the cost. The fineness modulus of medium sand is 2.6 and the maximum particle size is 5 mm. To acquire the ideal workability, high active admixture "SBT®-HDC(V) UHPC" was added in the mixture. Considering the bridge effect of fiber in UHPC, two kinds of high strength steel fibers, end-hooked fiber (type I) and straight fiber (type II) were added with a volume fraction of 2% in UHPC specimens.

According to GB 50010-2010 (2010), the cubic specimen with a size of 100 mm × 100 mm× 100 mm, dog

(a) Tensile coupons test

(b) Compressive coupons test

Fig. 1 The compression and tension tests of UHPC

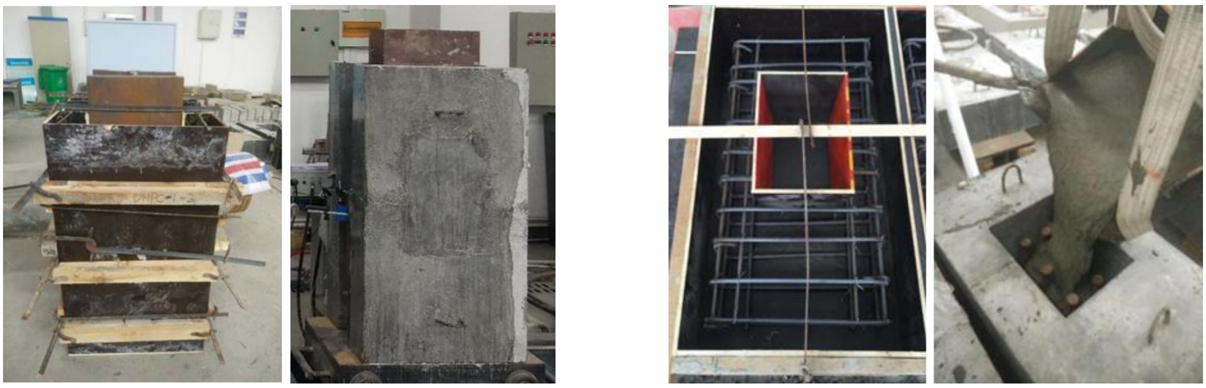

(a) Forming method of NSG and UHPCG (b) Forming method of NSF

Fig. 2 Forming method of specimens

Table 3 Test specimens and details of test variables

Specimen	Number	Shear pocket	h_{stud} (mm)	d_{stud} (mm)	h_{stud}/d_{stud}
NCG	3	\	150	30	5
NCF	3	UHPC	150	30	5
UHPCG	3	\	150	30	5

Note: d_{stud} is the diameter of the headed stud; h_{stud} is the height of the headed stud

bone specimens with a size of 100 mm × 100 mm × 500 mm, and the prism specimens with a size of 100 mm× 100 mm× 300 mm were cast to test the compressive strength, direct tensile strength and the elastic modulus, respectively. The compression and tension tests are shown in Fig. 1, and test results are presented in Table 2. Besides, the slump flow values of UHPC using in this paper is 615 mm.

2.2 Specimens details

The specimen with large-headed studs embedded in the NSC slab, UHPC slab, and the UHPC shear pocket was labeled as NCG, UHPCG, and NSF, respectively. The slab of NCG and UHPCG was molded one-time, as shown in Fig. 2(a). However, the slab of NCF, which includes a shear

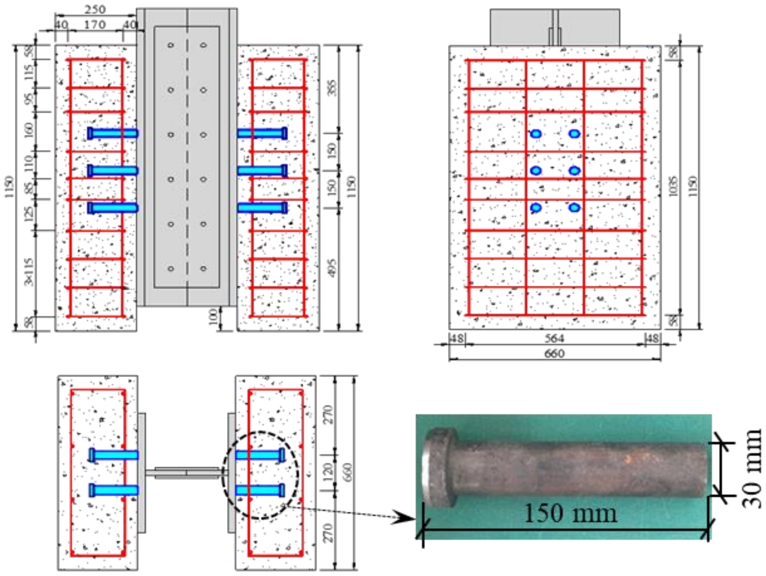

(a) The concrete slab was molded one time

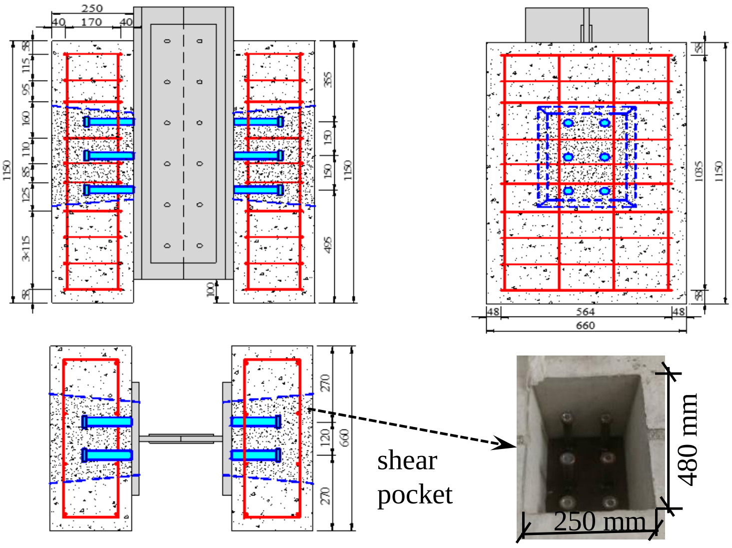

(b) The concrete slab with UHPC shear pocket

Fig. 3 Details of specimens (unit: mm)

pocket, was cast in two steps. The forming and pouring process of the specimen NCF is shown in Fig. 2(b). Test parameters and the specimen dimension are shown in Table 3.

In order to ensure the accuracy, three specimens of the same group were poured simultaneously. The details and dimensions of push-out specimens are presented in Fig. 3. It deserves to be mentioned that the diameter of studs in the research is 30mm, which is larger than that of the normal headed stud. The aspect ratio of the large-headed stud is 5, and the yield strength is 385.4 MPa, as shown in Fig. 4. The dimension of the H-shaped steel beam is 250 mm×250 mm×14 mm×14 mm, of which yield strength in tension is 387.0 MPa. The diameter of the steel bar is 8 mm with a tensile strength of 328.5 MPa, their arrangement is shown in Fig. 3.

2.3 Test setup and procedure

All push-out specimens were tested under uniaxial loading, as shown in Fig. 5. The measurement range of the testing machine is varied from 0 to 500 kN. A spreading plate was placed on the top of the steel beam to avoid the stress concentration. Before testing, the specimen was preloaded. During testing, the load was applied with an increment of 10 kN during the loading process. The interlayer slip between the steel beam and concrete slab was recorded by the dial indicators attached to the concrete slabs and steel girder. The maximum range of the dial gauge was 15 mm which was mostly beyond the ultimate slip.

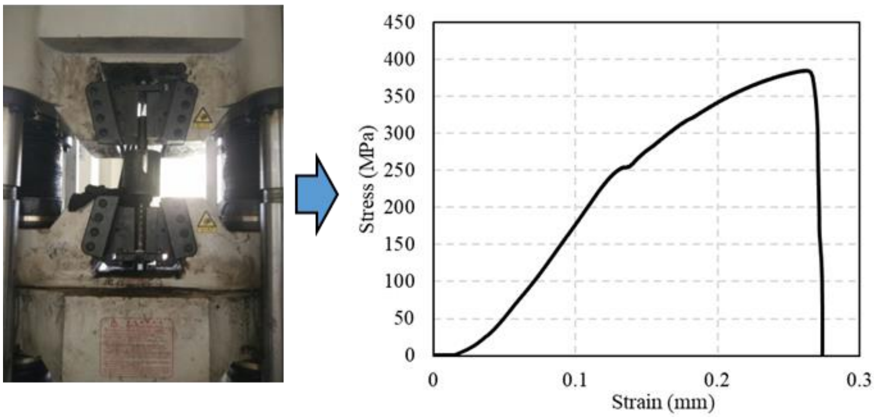

Fig. 4 The stress-strain curve of the stud in the tensile testing

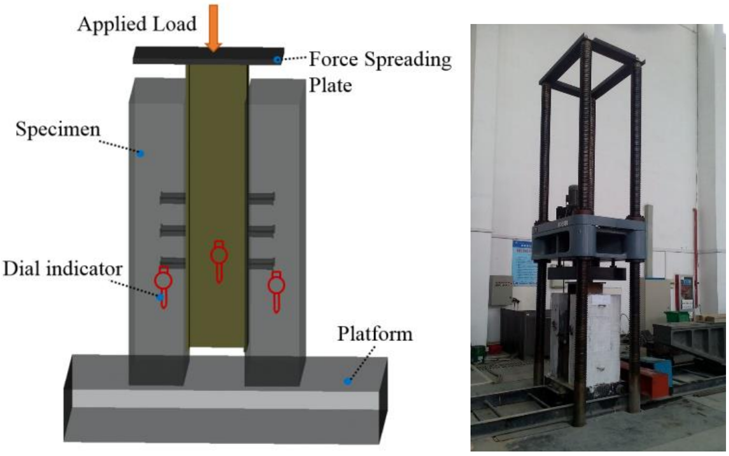

Fig. 5 Test setup

3. Test results

3.1 Failure mode and crack pattern

The failure mode of push-out specimens is affected by many parameters. According to the previous study (Xue *et al.* 2008, Qi *et al.* 2017b), three kinds of failure modes including concrete failure, shank failure, and combined failure of concrete failure and shank failure usually occurs for steel-concrete composite structures. In this study, the shank failure occurred for the UHPCG, the concrete failure combined with shank failure occurred for the NCG and NCF. For specimen NCG, diagonal cracks and splitting cracks occurred on the surface of the concrete slab, as shown in Fig. 6. However, only the local concrete spalling was observed on the surface of the UHPC slab, indicating that the high tensile and compressive strength of UHPC is beneficial for resisting crack formation and development. The addition of 1% to 2% steel fibers by volume is essential, attributing the reason that the bridging effect of steel fibers in UHPC is also beneficial for resisting the splitting cracks and improving the ductility of structures (An *et al*. 2017, Wang *et al.* 2019).

Besides, it should be noted that the crack distribution on the slab surface of NCF is different from that of UHPCG and NCG. Regarding to the NCF, the diagonal cracks initiated from the interface between UHPC and normal concrete, and then cracks propagated into the concrete slab. At the failure load, it can be found that the concrete crushing occurred on the bottom surface of the shear pocket. The result indicates that the interface between UHPC and concrete is weak due to the discontinuities of steel fibers and bad bonding capability, and that the existence of the interface is disadvantageous for the improvement of shear resistance.

3.2 Shear resistance

The experimental results of the ultimate strength per stud (average values), interfacial slip, and the failure mode are summarized in Table 4. It is found that the shear resistance of UHPCG is 11.4% and 5.5% higher than that of NCG and NCF, respectively. Besides, the shear resistance of NCF increased by 5.5% in comparison with the NCG. The experimental results indicate that the excellent mechanical property of UHPC, such as high tensile strength and

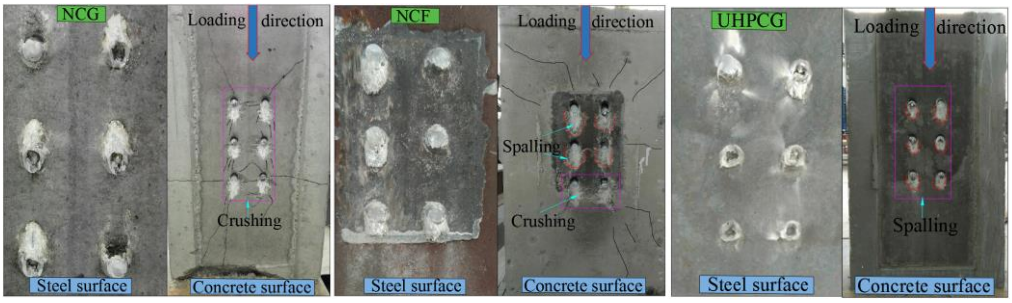

Fig. 6 Failure modes of specimens

Table 4 Summary of test results

Specimen	P_u (kN)	S_u (mm)	S_{max} (mm)	Failure mode
NCG	318.0	10.3	10.6	Shank failure & Concrete splitting
NCF	335.6	6.7	7.7	Shank failure & Concrete splitting
UHPCG	354.1	5.8	6.7	Shank failure

Note: P_u = ultimate strength per stud; S_u = interfacial slip corresponding to peak load; S_{max} = ultimate slip

Table 5 Shear stiffness

Specimen	Slip at 0.2 mm			Slip at 2 mm		
	load (kN)	slip (mm)	k_1 (kN·mm^{-1})	load (kN)	slip (mm)	k_2 (kN·mm^{-1})
NCG	33	0.2	165	229.2	2	114.6
NCF	41.5	0.2	207.5	261.6	2	130.8
UHPCG	55.6	0.2	278.0	278.8	2	139.4

modulus of elasticity, is beneficial for improving the shear strength of the large-headed stud. Regarding to the ultimate slip, it can be found that the ultimate slip of NCG, NCF and UHPCG is 10.6 mm, 7.7 mm and 6.7 mm, respectively, indicating the high compressive strength and elastic modulus of UHPC is disadvantageous for improving the plastic deformation capacity of the stud.

3.3 Shear load-slip curve

The shear load-slip curve is an important characteristic for the ultimate limit state analysis of the composite beams. The shear load-slip curves of all specimens are plotted in Fig. 7. Through comparing the three groups of load-slip curves, it can be found that all the load-slip curves comprise two stages: a linear elastic stage and a plastic stage. Approximate linear behavior is observed when the slip is less than 2 mm. On a slip of 2 mm, the load of NSG, NSF, and UHPCG is 229.2 kN, 261.6 kN, and 278.8 kN, respectively, accounting for about 70% of the ultimate strength. The shear stiffness gradually decreases when the slip is greater than 2 mm.

In addition, it can be clearly observed in Fig. 7 that the ultimate slip of UHPCG, NCF, and NCG is different. The ultimate slip of NCG is 10.6 mm, which is 58% higher than that of UHPCG. The NCF has the medium ultimate slip comparing to NCG and UHPCG. According to the definition of ductility and considering the shape of load-slip curves, it can be inferred from the experimental results that the ductility decrease when the large-headed stud embedded in a UHPC.

3.4 Shear stiffness

Table 5 summarizes the stiffness of NCG, NCF, and UHPCG. Currently, a lot of methods were proposed to calculate the shear stiffness for headed stud. Qi *et al.* (2017b) recommended the shear stiffness be defined as the secant slope of the load-slip curve at a relative slip of 0.2 mm and 2 mm. It can be seen from Table 5 that the stiffness of UHCG is 32.1% and 21.6% higher than the NCG, respectively when the slip is 0.2 mm and 2 mm, respectively. The stiffness of NCF is larger than NCG, but is smaller than that of UHPCG. The results indicate that the high elastic modulus of UHPC is advantageous to improve the stiffness of headed stud.

4. Finite element analysis

4.1 FE model establishment and verification

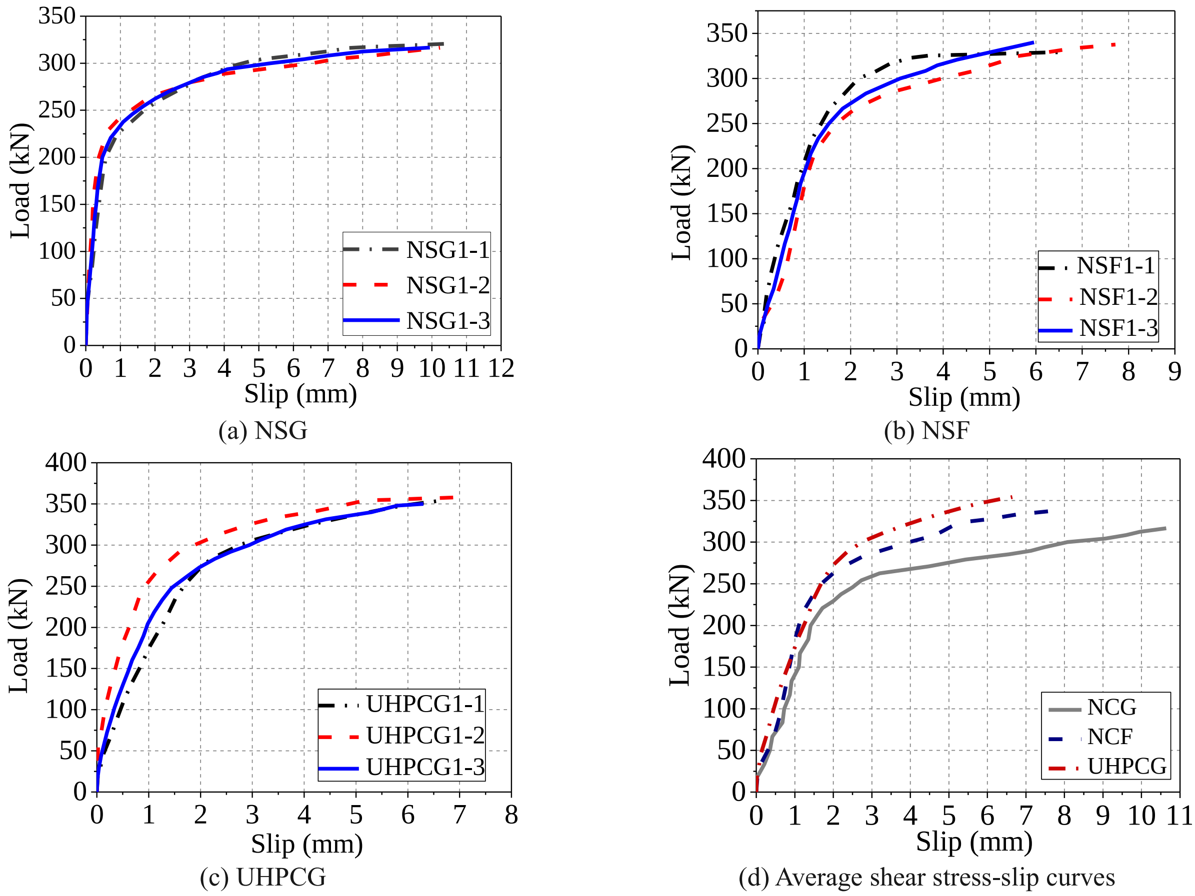

Fig. 7 Load-slip curves of test specimens

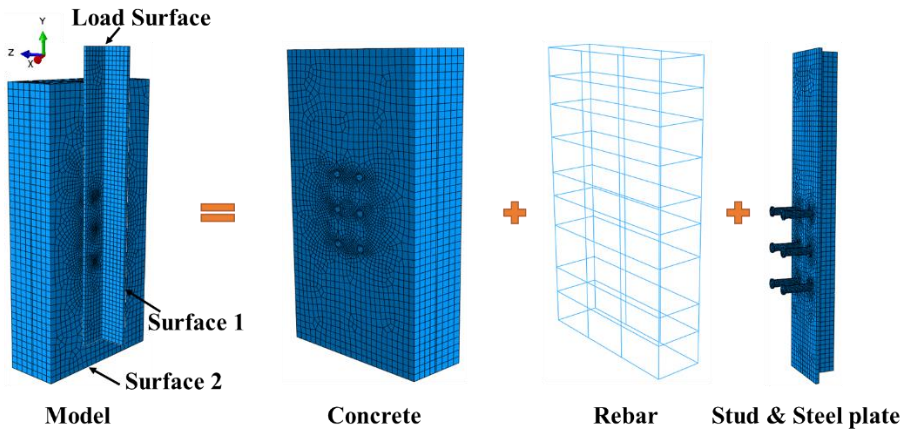

Fig. 8 FE model

4.1.1 Model setup

The numerical analysis was carried out using the ABAQUS. The FE model was established with the consideration of material, interaction and geometric non-linearity (Han *et al*. 2017). Due to the symmetry of the geometry of the specimen, loading method, and the boundary condition, only half of the actual push-out specimen was modeled. For modeling the steel beam, concrete, and stud, the solid element C3D8R was introduced. The linear truss element (T3D2) was adopted to approach the behavior of the steel bar (Liu *et al.* 2016). The surface-to-surface contact interaction was applied to simulate the physical behavior of interlayer between the stud and concrete slab, steel beam and concrete slab. In

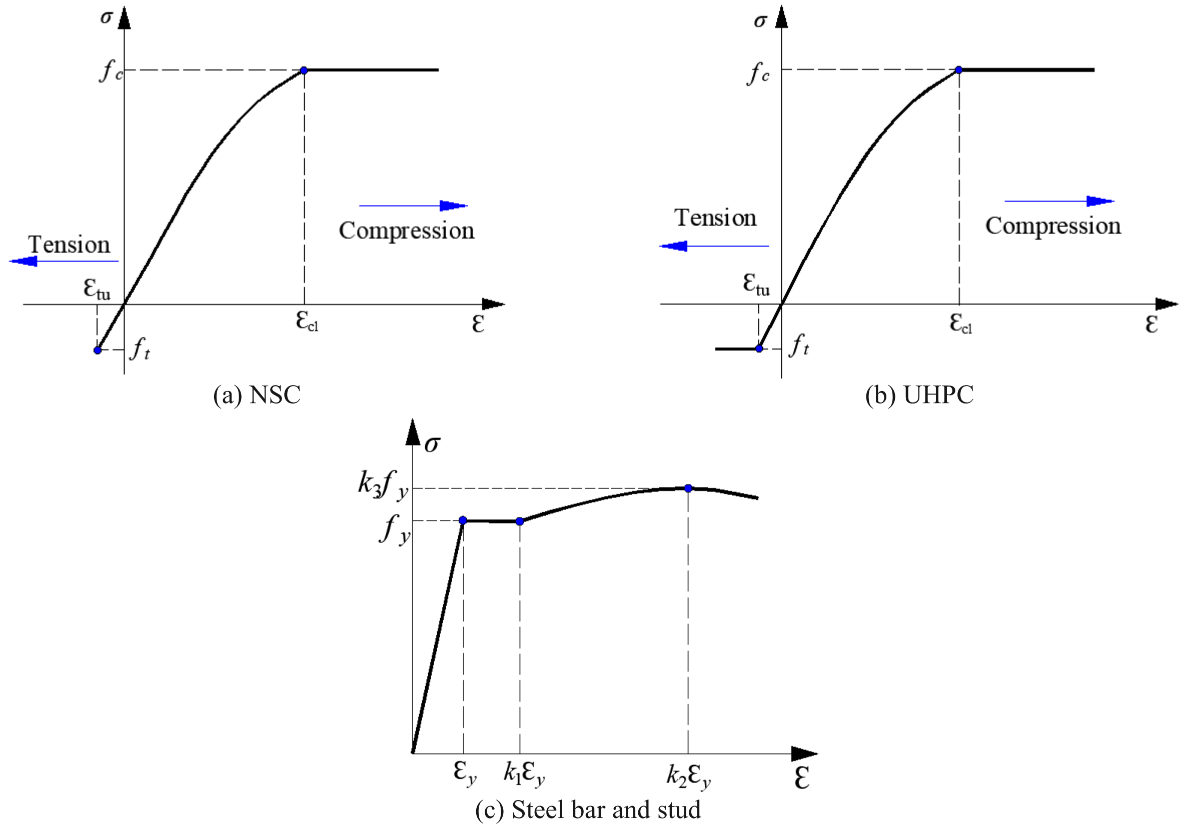

Fig. 9 Material constitutive model

order to simulate the behavior of contact interaction, the penalty contact method was used to serve as a mechanical constraint formula. Perfect bond between concrete and reinforcement through the embedded method (Xu *et al.* 2016). In addition, the HARD contact property, which well-suited for illustrating the normal behavior of the interface plane was chosen. The mesh scale for concrete slab, steel beam, and stud was different, the overall mesh scale was 25 mm approximately (Wang *et al.* 2019), while the smallest mesh scale was about 3 mm (Nguyen *et al.* 2009). The coordinate system and the overviews of the FE model were shown in e Fig. 8.

4.1.2 Boundary and loading condition

The constraint conditions should be defined for every component when all components of the model were assembled. In this study, the bottom of the concrete slab (surface 2) was restrained from moving in all three directions with the consideration of the actual load situation. Symmetry boundary condition was applied to surface 1 which was symmetric in the X-axis. The uniaxial displacement load along Y direction was applied to the all-nodes belonging to the loading surface. To obtain an accurate solution, the loading rate of 0.02 mm/s in the vertical direction was adopted in this research according to Qi *et al.* (2018).

4.1.3 Material modelling

According to the experimental data of material, the nonlinear numerical analysis was carried out in this research. A combined damage-plasticity (CDP) model was used with consideration of compressive behavior and tensile behavior of concrete. The stress-strain relationship of UHPC in tension and compression was selected based on Qi *et al.* (2019), as shown in Figs. 9(a) and 9(b). For the stress-strain relationship, ε_{cl} is the strain at maximum compressive stress, ε_{tu} is the strain at maximum tensile stress, it is selected according to Wang *et al.* (2019) and Qi et al. (2017). To simulate the damage evolution process, the damage variable was defined. According to Cao *et al.* (2019), concrete damage index can be calculated as

$$D = 1 - \sqrt{\frac{\sigma}{E_c \varepsilon}} \tag{1}$$

The plasticity parameters of UHPC including the dilation angles of 56 degrees, flow potential eccentricity of 0.1, *k* of 0.66, Poisson's ratio of 0.2 and ratio of the biaxial/uniaxial compressive strength ratio of 1.16 are set for this CDP model (Shafieifar *et al.* 2017, Wang *et al*. 2019, An *et al.* 2019). The plasticity parameters of normal strength concrete including the dilation angles of 38 degrees, flow potential eccentricity of 0.1, *k* of 0.66, Poisson's ratio of 0.19 and ratio of the biaxial/uniaxial compressive strength ratio of 1.16 are set for this CDP model (Jankowiak *et al.* 2005).

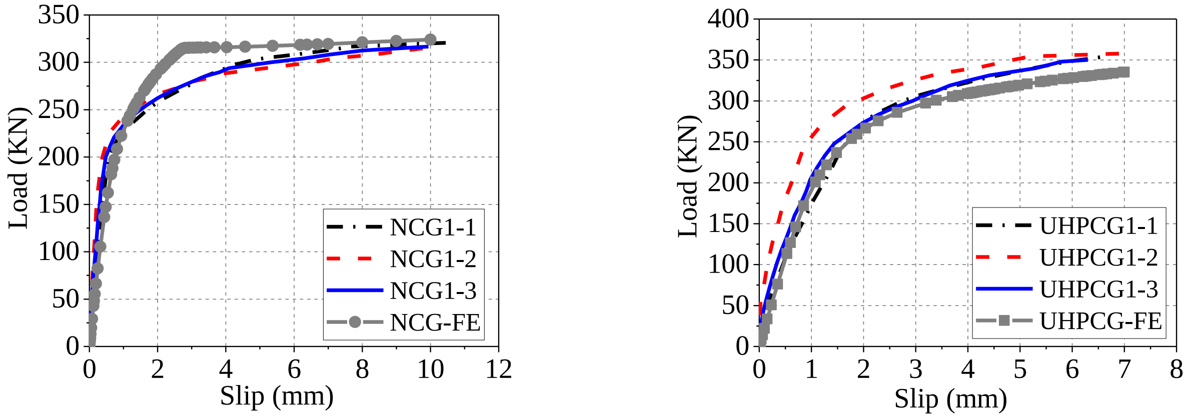

Fig. 10 Comparison of the load-slip curves from the test results and the FEM model results

The push-out tests in this study showed that the steel beam and steel bar were not damaged. Consequently, the steel plates and steel bars were defined according to Shao *et al.* (2005), without considering the damage in the numerical simulation, as shown in Fig. 9(c). However, the headed stud was defined with consideration of damage, the damage index is defined according to Cao *et al*. 2019, and the fracture strain of the headed studs was defined as the plastic strain at the ultimate state. According to Esmaeily and Xiao (2005), their stress-strain stage in the hardening stage can be expressed as

$$\sigma = k_3 f_y + \frac{E_s(1-k_3)}{\varepsilon_y(k_2-k_1)^2}(\varepsilon - k_2\varepsilon_y)^2 \tag{2}$$

In this study, the values of k_1, k_2, and k_3 are selected as 12, 120, and 1.4, respectively, as suggested by Han *et al.* (2019). The ε_y is taken as 2000 μm/m.

4.1.4 Verification

The verification was carried out to prove the accuracy of numerical results. As shown in Fig. 10, the results of load-slip curves produced by the simulation agree well with the experimental results. Thus, it can be believed that the results of numerical simulation of the push-out tests is reliable and accurate, and that the parametric analysis can be carried out using the proposed FE model.

4.2 Parametric analysis

To further investigate the shear behavior of the large-headed stud shear connectors in UHPC, the parametric analysis was conducted based on the FE model of UHPCG. The aspect ratio of stud, compressive strength of UHPC, and the diameter of stud were considered as crucial parameters. In addition, the layout of the stud including spacing of stud was studied. The input FEA parameters are shown in Table 6.

4.2.1 Concrete strength

For illustrating the influence of concrete strength on the shear behavior of headed stud, four different strength grades of UHPC with 80 MPa, 120 MPa, 180 MPa, and 200 MPa were studied. The tensile strength and elastic modulus inputted in the FE model were obtained according to the FHWA-HRT-06-103 (2006), as shown in Table 6. The shear-slip curves are presented in the Fig. 11(a). Obviously, the stiffness increases with the increase of the concrete strength, whereas an increase in concrete strength did not increase the shear resistance of headed stud, attributing the reason that the shank failure mode controls the shear capacity of the large-headed stud.

4.2.2 Stud diameter

To investigate the shear behavior of the large-headed stud embedded in the UHPC slab, the stud diameter is designed from 22 mm to 40 mm. Fig. 11(b) presents the load-slip curve of the FE results. It is found that the shear stiffness and resistance increase with the increase of the stud diameter. The shear resistance increase by 20% when the stud diameter increases from 20 mm to 40 mm. Besides, it can be found that the growth of shear resistance is linear to the increase of stud diameter.

4.2.3 Aspect ratio

The current specifications specifies that the aspect ratio of the stud should not be smaller than 4 in steel-concrete composite structures. However, a previous study has proven that the stud with the aspect ratio of 2.3 can develop a full shear strength, when it is embedded in the UHPC slab (Wang *et al*. 2019). According to the load-slip curves obtained in the FE analysis (see Fig. 11(c)), no obvious difference is observed, indicating that the aspect ratio has little effect on the shear resistance and shear stiffness when the aspect ratio is larger than 2.

4.2.4 Spacing of the stud

The spacing of stud in the direction of shear force is determined by the shear resistance and shear load-slip curve according to the research by Ollgaard *et al.* (1971). The values of the spacing ranged from 2 d to 7 d were studied in the FE analysis. It can be found in Fig. 11(d) that the shear resistance decrease by 8.1% when the spacing of studs in the direction of the shear force decrease from 5 d to 2d. However, no obvious difference can be found when the spacing decreases from 5 d to 3 d, indicating that 3d is

Table 6 FEA parameters

Series	*d* (mm)	Aspect ratio	S_p	f_c (MPa)	f_t (MPa)	E_c (mm)	f_u (MPa)
U80	30	5	4*d*	80	5.0	34.3	500
U120	30	5	4*d*	120	6.1	42.0	500
U180	30	5	4*d*	180	7.5	51.4	500
U200	30	5	4*d*	200	7.9	54.2	500
U22	22	5	4*d*	124	6.7	45.4	500
U30	30	5	4*d*	124	6.7	45.4	500
U35	35	5	4*d*	124	6.7	45.4	500
U40	40	5	4*d*	124	6.7	45.4	500
U-2	30	2	4*d*	124	6.7	45.4	500
U-4	30	4	4*d*	124	6.7	45.4	500
U-5	30	5	4*d*	124	6.7	45.4	500
U-7	30	7	4*d*	124	6.7	45.4	500
Gu-2d	30	5	2*d*	124	6.7	45.4	500
Gu-3d	30	5	3*d*	124	6.7	45.4	500
Gu-4d	30	5	4*d*	124	6.7	45.4	500
Gu-5d	30	5	5*d*	124	6.7	45.4	500
Gu-7d	30	5	7*d*	124	6.7	45.4	500
Gu-10d	30	5	10*d*	124	6.7	45.4	500

Note: S_p = the spacing between studs in the direction of shear force; f_u = the tensile strength of stud

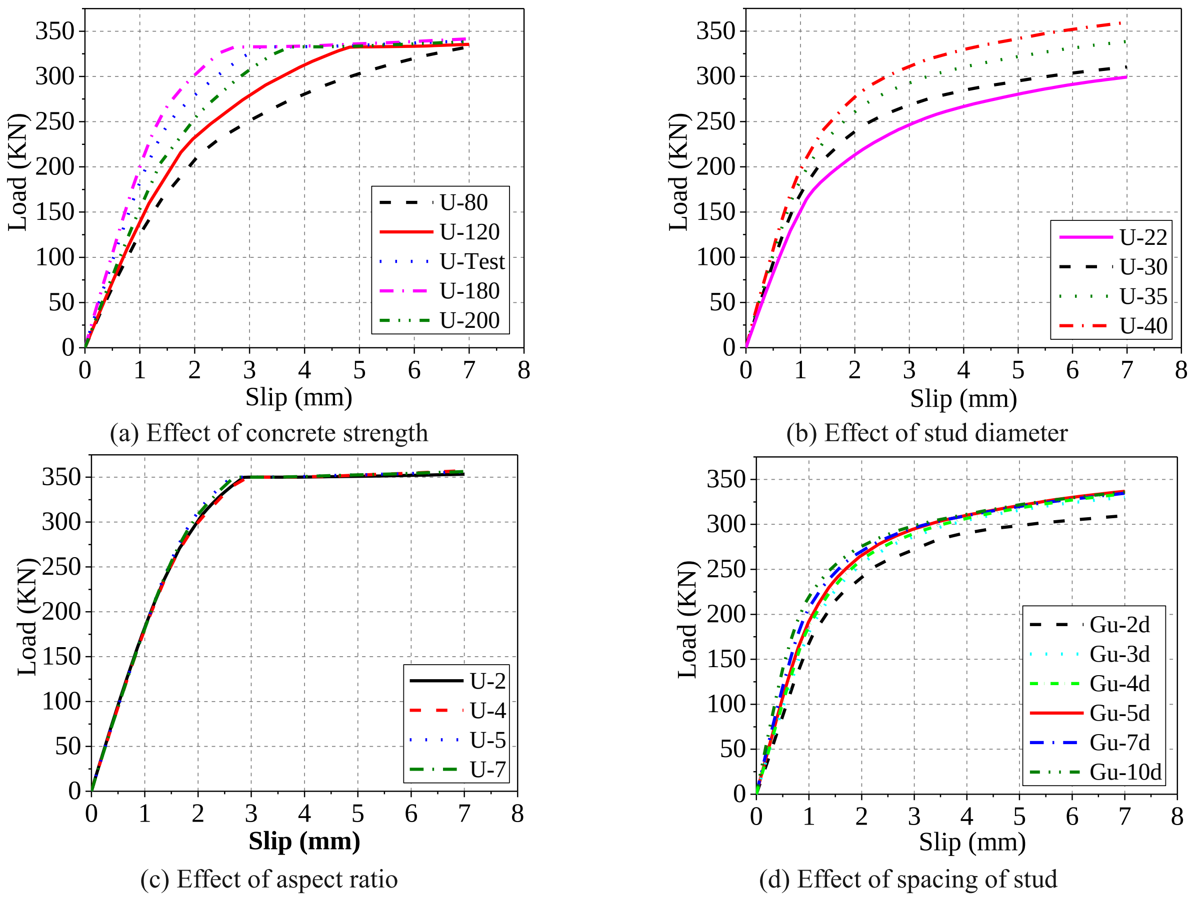

(a) Effect of concrete strength

(b) Effect of stud diameter

(c) Effect of aspect ratio

(d) Effect of spacing of stud

Fig. 11 Load-slip curves of the parametric study

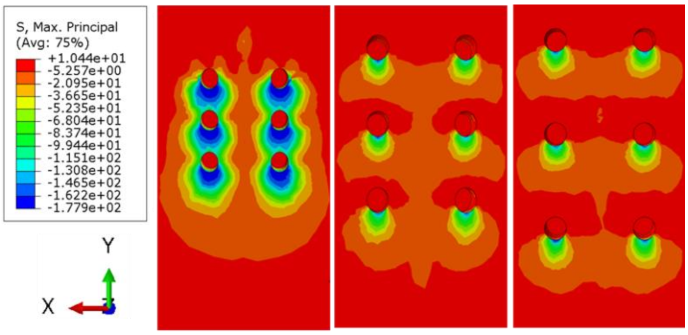

Fig. 12 Maximum principal stress distribution of UHPC slab

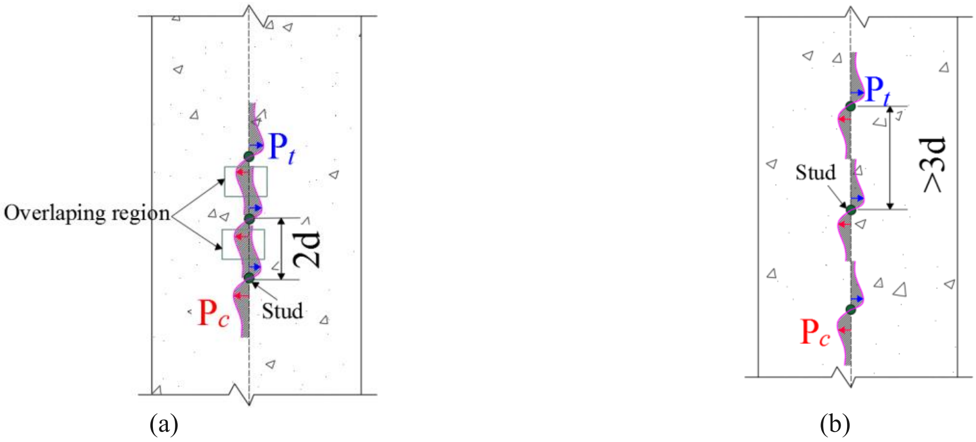

Fig. 13 Stress distribution on the surface of slab

fulfilled to develop the full shear resistance. Fig. 12 presents the maximum principal stress distribution of UHPC slab when the spacing of the stud varied from 2 d to 4 d. It can be found that the influence of the interaction between two studs cannot be neglected when the spacing of the stud is 2 d. Through the concept analysis, it can be found that no overlap of the stress occurs when the spacing of studs is larger than 3 d, as shown in Fig. 13. It is recommended that the spacing of studs in the direction of the shear force should be larger than 3 d when the large-headed stud is embedded in UHPC.

5. Proposed equations for shear Load-Slip curve and shear resistance

5.1 Shear load-slip behavior

The load-slip curves of UHPC specimens exhibit a brittle behavior according to Fig. 7. Thus, it is necessary to derive the simplified load-slip curve considering the mechanical properties of UHPC for the stud shear connectors embedded in the UHPC. Table 7 presents the empirical formulas which have been proposed to predict the static behavior of push-out specimens by previous researchers.

Based on the 9 push-out tests and previous studies, the expression of the load-slip relationship is given by

$$\frac{P}{P_u} = \frac{S}{0.2 + S} \tag{3}$$

where P denotes the shear load of per stud, S denotes the slip, and P_u denotes the ultimate shear load.

Comparing the Eq. (1) with previous equations, it is found that the proposed equation matches well with the load-slip curve of the specimens used in this study and the previous study (Wang *et al.* 2018; Wang *et al.* 2019), as shown in the Fig. 12. The results indicate that Eq. (3) gives a better estimation of load-slip relationships.

5.2 Shear resistance

Currently, the formula, which is applicable to normal steel-concrete composite structure, is usually used to predict the shear resistance of headed stud embedded in UHPC. However, it is found that these formulas underestimate the shear resistance of the stud in steel-UHPC composite structure according to previous research (Kruszewski *et al.* 2018, Cao *et al*. 2017, Wang *et al.* 2019). Therefore, a reasonable calculation method should be established to evaluate the shear resistance for headed studs embedded in UHPC.

According to current research, the shear resistance of headed stud embedded in UHPC is governed by the shank

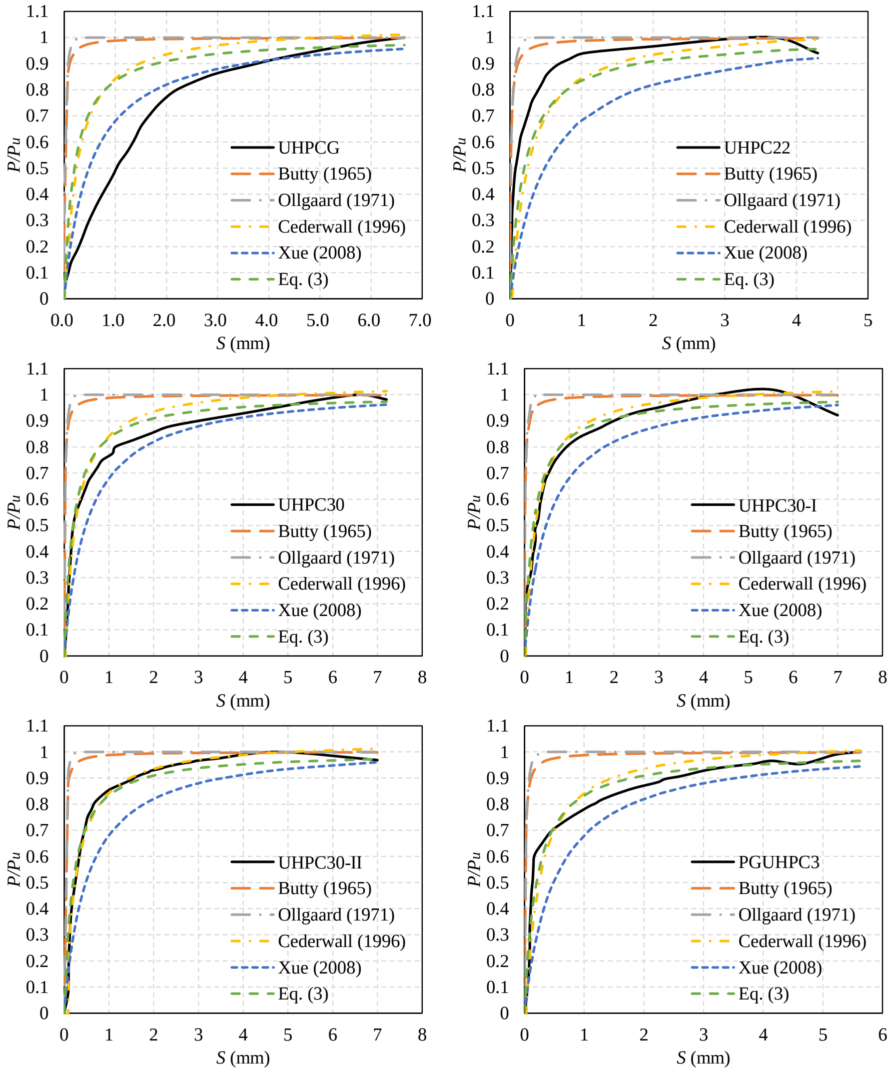

Fig. 14 Comparison of expressions of load-slip relationship

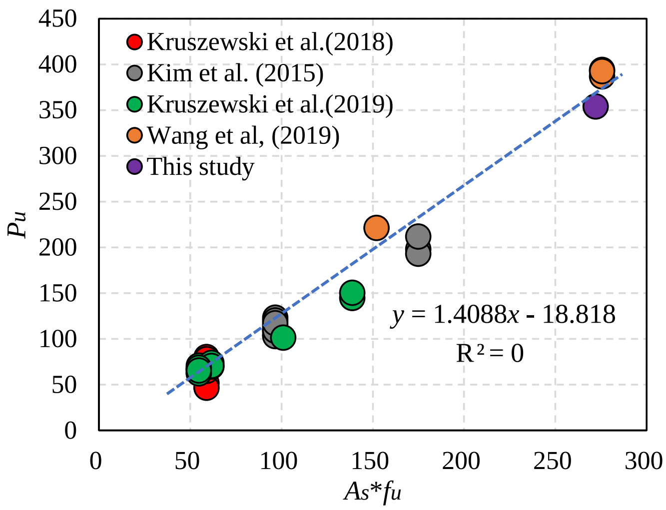

Fig. 15 Ultimate strength of headed studs

Table 7 Proposed equations of load-slip relationship

Author	Equations	
Buttry (1965)	For normal strength concrete	$\frac{P}{P_u}=\frac{80S}{1+80S}$
Ollgaard *et al.* (1971)	For normal strength concrete	$\frac{P}{P_u}=(1-e^{-18S})^{0.4}$
Cederwall (1996)	For normal strength concrete	$\frac{P}{P_u}=\frac{2.24(S-0.058)}{1+1.98(S-0.058)}$
	For high performance concrete	$\frac{P}{P_u}=\frac{4.44(S-0.031)}{1+4.24(S-0.031)}$
Xue *et al.* (2008)	Single stud of concrete	$\frac{P}{P_u}=\frac{S}{0.5+0.97S}$

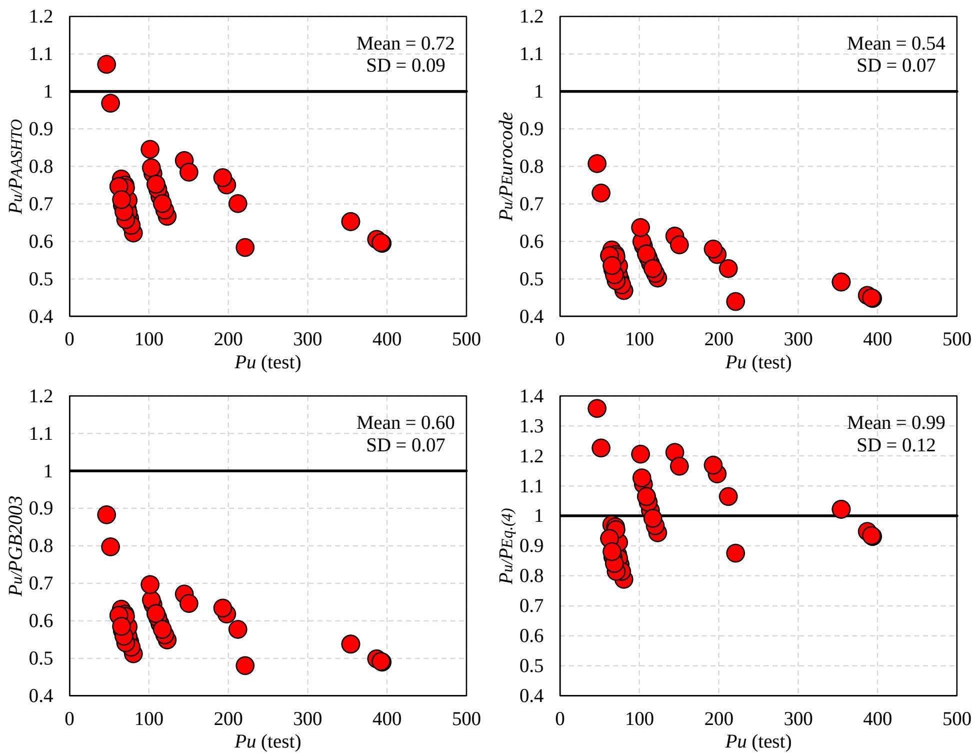

Fig. 16 Comparisons between test result and calculated results

failure, which is different from that embedded in normal strength concrete. To obtain the shear strength of stud embedded in UHPC, the test results of Wang *et al.* (2019), Kruszewski *et al.* (2018a), Kruszewski *et al.* (2018b), Kim *et al.* (2015), and this study were regressed using the shear resistance model in current design codes. The results of the regression analysis were shown in Fig. 15. Based on the result of the regression analysis, the shear resistance of headed stud embedded in UHPC can be calculated as

$$P_u=1.4A_sf_u-19 \tag{4}$$

where A_s is sectional area of the studs; f_u is tensile strength of the studs.

The formulas calculating the shear strength of headed stud in AASHTO LFRD (2014), Eurocode4 (2005), and GB50017-2003 (2003) were listed in Table 8. To verify the accuracy of the Eq. (4), the shear strength results calculated using Eq. (4) were compared with that calculated results, which are obtained according to the above design codes. The comparison results were listed in Table 9. Fig 16 shows the calculation results of Eq. (4) matches well with the experimental results, indicating that the proposed equation is applicable to predicate the shear resistance for headed stud embedded in the UHPC slab.

It should be clarified that the shear resistance for headed studs embedded in the UHPC shear pocket is improved according to this study. However, it is found that the formula proposed above is not suitable for them. Some tests and research will be carried out in the future.

Table 8 The shear strength formula in design codes

AASHTO LRFD (2014)	$P_u = \phi 0.5 A_s \sqrt{E_c f_c}/\gamma_v \leq \phi A_s f_u/\gamma_v$
Eurocode4 (2001)	$P_u = 0.29 \alpha d^2 \sqrt{E_c f_c}/\gamma_v \leq 0.8 A_s f_u/\gamma_v$
GB50017-2003 (2003)	$P_u = 0.43 A_s \sqrt{E_c f_c} \leq 0.7 A_s f_u$

Table 9 Comparisons between the test result and calculated results

Ref.	Specimens	P_u (kN)	P_u/Eq. (4)	P_u/P_{AASHTO}	$P_u/P_{Eurocode\ 4}$	$P_u/P_{GB500017\text{-}2003}$
This study	UHPCG	354.1	1.02	0.65	0.49	0.54
Kruszewski *et al.* (2018)	UHPC-A_heat	68.2	0.93	0.73	0.55	0.60
	UHPC-B	51.6	1.23	0.97	0.73	0.80
	UHPC-C	72.7	0.87	0.69	0.52	0.57
	UHPC-D	75.6	0.84	0.66	0.50	0.54
	Side-Cov_25 mm	46.6	1.36	1.07	0.81	0.88
	Side-Cov_50 mm	68.4	0.93	0.73	0.55	0.60
	Side-Cov_60 mm	69.6	0.91	0.72	0.54	0.59
	Paint	65.2	0.97	0.77	0.58	0.63
	Unbonded	73.8	0.86	0.68	0.51	0.56
	V.ferrule	80.3	0.79	0.62	0.47	0.51
	Vibration	77.7	0.81	0.64	0.48	0.53
Kim *et al.* (2015)	UHPC-1-A	198.0	1.14	0.75	0.56	0.62
	UHPC-1-B	193.0	1.17	0.77	0.58	0.63
	UHPC-1-C	212.0	1.06	0.70	0.53	0.58
	UHPC-2-A	123.0	0.94	0.67	0.50	0.55
	UHPC-2-B	120.0	0.97	0.68	0.51	0.56
	UHPC-2-C	114.0	1.02	0.72	0.54	0.59
	UHPC-3-A	105.0	1.11	0.78	0.59	0.64
	UHPC-3-B	103.0	1.13	0.80	0.60	0.66
	UHPC-3-C	111.0	1.05	0.74	0.56	0.61
	UHPC-4-A	109.0	1.06	0.75	0.57	0.62
	UHPC-4-B	109.0	1.06	0.75	0.57	0.62
	UHPC-4-C	117.0	0.99	0.70	0.53	0.58
Kruszewski *et al.* (2019)	D12aS8-A1	66.7	0.86	0.70	0.52	0.57
	D12aS8-A2	62.3	0.92	0.75	0.56	0.61
	D12bS8-A3	69.8	0.96	0.75	0.56	0.62
	D12aS8-A4	70.7	0.81	0.66	0.50	0.54
	D12aS4-A5	66.7	0.86	0.70	0.52	0.57
	D12bS8-A6	73.8	0.91	0.71	0.53	0.58
	D12bS8-A7	70.5	0.95	0.74	0.56	0.61
	D12aS8-B1	68.5	0.84	0.68	0.51	0.56
	D12aS8-C1	62.3	0.92	0.75	0.56	0.61
	D16S4-D1	101.4	1.21	0.85	0.64	0.70
	D19aS4-D2	144.6	1.21	0.82	0.61	0.67
	D19aS4-D3	150.3	1.17	0.78	0.59	0.65
	D12aS8-E1	65.4	0.88	0.71	0.54	0.59
Wang *et al.* (2019)	UHPC22	221.3	0.88	0.58	0.44	0.48
	UHPC30	387.0	0.95	0.61	0.46	0.50
	UHPC30-I	393.8	0.93	0.59	0.45	0.49
	UHPC30-II	392.5	0.93	0.60	0.45	0.49
Mean	/	/	0.99	0.72	0.54	0.60
SD	/	/	0.13	0.09	0.07	0.07

6. Conclusions

In this study, the push-out test and numerical simulation were implemented to study the static behavior of the grouped large-headed stud, which is embedded in UHPC slab, UHPC pocket, and normal strength concrete (NSC) slab. The following conclusions could be drawn from the present study:

- The results of the push-out test indicate that the shear resistance of the headed stud, which is embedded in UHPC slab and UHPC shear pocket, is improved when compared with that embedded in normal strength concrete. It is found that the shear resistance of UHPCG is 11.4% and 5.5% higher than that of NCG and NCF, respectively.
- The results of numerical analysis indicated that both shear stiffness and resistance increased with the increase of stud diameter when the stud diameter varied from 22 mm to 40 mm. Moreover, the growth of the shear resistance of the large-headed stud is approximately linear to the increase of stud diameter.
- Based on the failure model of the push-out specimens and the mechanical properties of UHPC, the formula for predicting the shear resistance of headed stud, which is embedded in the UHPC slab, is proposed. Comparing the proposed formula with that in AASHTO LRFD (2014), Eurocode 4 (2005) and GB50017-2003, it is found that the proposed equation matches well with the experimental results.
- An empirical load-slip formula is proposed to predict the load-slip relationship of grouped large-headed stud embedded in the UHPC slab. The comparison indicates that the proposed formula matches well with the load-slip curve of the specimens tested in this study and previous study.
- In the arrangement of grouped large-headed stud, the overlap of the stress occurs due to the interaction between two studs when the spacing of studs in the direction of the shear force is smaller than 3 d, resulting in the reduction of the shear resistance. It is recommended that the spacing of studs in the direction of the shear force should be greater than 3 d in the arrangement of stud for steel-UHPC composite structures.

Acknowledgements

This study was supported by the Joint Funds of National Natural Science Foundation of China (U1934205) and the National Key R&D Plan (2017YFC0703402). The financial support is gratefully appreciated.

Declaration of interests

Declarations of interest: none.

CRediT author statement

Yuqing Hu: Conceptualization, Methodology, Writing-Original draft preparation..

Guotang Zhao: Laboratory work support and Supervision.

Zhiqi He: Validation, Conceptualization and Data curation.

Jianan Qi: Writing-Reviewing and Editing.

Jingquan Wang: Conceptualization, Supervision, Funding acquisition, Laboratory work support.

Data availability

Some or all data, models, or code generated or used during this study are available from the corresponding author by request.

References

AASHTO (2014), AASHTO LRFD Bridge Design Specifications, American Association of State Highway and Transportation Officials; Washington, DC, USA.

An, L. and Cederwall, K. (1996), “Push-out tests on studs in high strength and normal strength concrete”, *J. Constr. Steel Res.*, **36**(1), 15-29. https://doi.org/10.1016/0143-974X(94)00036-H.

An, L.H. and Fehling, E. (2017), “Influence of steel fiber content and type on the uniaxial tensile and compressive behavior of UHPC”, *Constr. Build. Mater.*, **153**, 790-806.

Badie, S.S., Tadros, M.K., Kakish, H.F., Splittgerber, D.L. and Baishya, M.C. (2002), “Large shear studs for composite action in steel bridge girders”, *J. Bridge Eng.*, **7**(3), 195-203. https://doi.org/10.1061/(ASCE)1084-0702(2002)7:3(195).

Bonilla, J., Bezerra, L.M., Mirambell, E. and Massicotte, B. (2018), “Review of stud shear resistance prediction in steel-concrete composite beams”, *Steel Compos. Struct.*, **27**(3), 355-370. https://doi.org/10.12989/scs.2018.27.3.355.

Buttry, K.E. (1965), “Behavior of stud shear connectors in lightweight and normal-weight concrete”, Ph.D. Dissertation, University of Missouri--Columbia, Rolla, USA.

Cao, J. and Shao, X. (2019), “Finite element analysis of headed studs embedded in thin UHPC”. *J. Constr. Steel Res.*, **161**, 355-368. https://doi.org/10.1016/j.jcsr.2019.03.016.

Cao, J., Shao, X., Deng, L. and Gan, Y. (2017), “Static and fatigue behavior of short-headed studs embedded in a thin ultrahigh-performance concrete layer”, *J. Bridge Eng.*, **22**(5), 04017005. https://doi.org/10.1061/(ASCE)BE.1943-5592.0001031.

Esmaeily, A. and Xiao, Y. (2005), “Behavior of reinforced concrete columns under variable axial loads: analysis”, *ACI Struct J.*, **102**(5), 736.

Eurocode 4 (2005), Design of composite steel and concrete structures, European Committee for Standardization; Brussels, Belgium.

Ganesh, P. and Murthy, A.R. (2019), “Tensile behaviour and durability aspects of sustainable ultra-high performance concrete incorporated with GGBS as cementitious material”, *Constr. Build. Mater.*, **197**, 667-680. https://doi.org/10.1016/j.conbuildmat.2018.11.240.

GB50010-2010 (2010), Code for design of concrete structures, China Building Industry Press; Beijing, China.

GB50017-2003 (2003), Code for design of steel structures, Ministry of Housing and Urban-Rural Development of China; Beijing, China

Graybeal, B.A. (2006), "Material property characterization of ultra-high performance concrete", No. FHWA-HRT-06-103; Faderal highway administration.

Hamoda, A., Hossain, K.M.A., Sennah, K., Shoukry, M. and Mahmoud, Z. (2017), "Behaviour of composite high performance concrete slab on steel I-beams subjected to static hogging moment", *Eng. Struct.*, **140**, 51-65. https://doi.org/10.1016/j.engstruct.2017.02.030.

Han, Q., Wang, Y., Xu, J., Xing, Y. and Yang, G. (2017), "Numerical analysis on shear stud in push-out test with crumb rubber concrete", *J. Constr. Steel Res.*, **130**, 148-158. https://doi.org/10.1016/j.jcsr.2016.12.008.

Hoang, ALe, Fehling, E. and Thai, D.K. and Nguyen, C.V. (2019), "Evaluation of axial strength in circular STCC columns using UHPC and UHPFRC", *J. Constr. Steel Res.*, **153**, 533-549. https://doi.org/10.1016/j.jcsr.2018.11.001.

Hoang, ALe, Fehling, E., Lai, B. and Thai, D.K. and Chau, N.V. (2019), "Experimental study on structural performance of UHPC and UHPFRC columns confined with steel tube", *Eng. Struct.*, **187**, 457-477. https://doi.org/10.1016/j.engstruct.2019.02.063.

Jankowiak, T. and Lodygowski, T. (2005), "Identification of parameters of concrete damage plasticity constitutive model", *Foundations of J. Environ. Civ.*, **6**(1), 53-69.

Kang, J.Y., Park, J.S., Jung, W.T. and Keum, M.S. (2014), "Evaluation of the shear strength of perfobond rib connectors in ultra-high performance concrete", *Engineering*, **6**(13), 989.

Kim, J.S., Kwark, J., Joh, C., Yoo, S.W. and Lee, K.C. (2015), "Headed stud shear connector for thin ultrahigh-performance concrete bridge deck", *J. Constr. Steel Res.*, **108**, 23-30.

Kruszewski, D., Wille, K. and Zaghi, A.E. (2018), "Design considerations for headed shear studs embedded in ultra-high performance concrete as part of a novel bridge repair method", *J. Constr. Steel Res.*, **149**, 180-194. https://doi.org/10.1016/j.jcsr.2018.07.015.

Kruszewski, D., Wille, K. and Zaghi, A.E. (2018), "Push-out behavior of headed shear studs welded on thin plates and embedded in UHPC", *Eng. Struct.*, **173**, 429-441. https://doi.org/10.1016/j.engstruct.2018.07.013.

Le, A.H., Ekkehard, F., Thai, D.K. and Nguyen, C.V. (2018), "Simplified stress-strain model for circular steel tube confined UHPC and UHPFRC columns", *Steel Compos. Struct.*, **29**(1), 125-138. https://doi.org/10.12989/scs.2018.29.1.125.

Lee, P.G., Shim, C.S. and Chang, S.P. (2005), "Static and fatigue behavior of large stud shear connectors for steel-concrete composite bridges", *J. Constr. Steel Res.*, **61**(9), 1270-1285. https://doi.org/10.1016/j.jcsr.2005.01.007.

Liu, X.P., Bradford, M.A., Chen, Q.J. and Ban, H.Y. (2018), "Finite element modelling of steel–concrete composite beams with high-strength friction-grip bolt shear connectors", *Finite Elem. Anal. Des.*, **108**(1), 623-634. https://doi.org/10.1016/j.finel.2015.09.004.

Luo, Y., Hoki, K., Hayashi, K. and Nakashima, M. (2015), "Behavior and strength of headed stud-SFRCC shear connection. I: Experimental study", *J Struct Eng.*, **142**(2), 04015112.

Nguyen, C.V., Le, A.H. and Thai, D.K. (2019), "Numerical simulation and analytical assessment of STCC columns filled with UHPC and UHPFRC", *Struct. Eng. Mech.*, **70**(1), 013-31. https://doi.org/10.12989/sem.2019.70.1.013.

Nguyen, H.T. and Kim, S.E. (2009), "Finite element modeling of push-out tests for large stud shear connectors", *J. Constr. Steel Res.*, **65**(10), 1909-1920. https://doi.org/10.1016/j.jcsr.2009.06.010.

Oehlers, D.J. and Park, S.M. (1992), "Shear connectors in composite beams with longitudinally cracked slabs", *J. Struct. Eng.*, **118**(8), 2004-2022. https://doi.org/10.1061/(ASCE)0733-9445(1992)118:8(2004).

Oehlers, D.J. and Sved, G. (1995), "Composite beams with limited-slip-capacity shear connectors", *J. Struct. Eng.*, **121**(6), 932-938. https://doi.org/10.1061/(ASCE)0733-9445(1995)121:6(932).

Ollgaard, J.G., and Slutter, R.G. and Fisher, J.W. (1971), "Shear strength of stud connectors in lightweight and normal-weight concrete", *AISC Eng. J.*, **8**(2), 55-64.

Qi, J., Hu, Y., Wang, J. and Li, W. (2019), "Behavior and strength of headed stud shear connectors in ultra-high performance concrete of composite bridges", *Front. Struct. Civ. Eng.*, **13**(5), 1138-1149. https://doi.org/10.1007/s11709-019-0542-6.

Qi, J., Wang, J., Li, M. and Chen, L. (2017b), "Shear capacity of stud shear connectors with initial damage: experiment, FEM model and theoretical formulation", *Steel Compos. Struct.*, **25**(1), 79-92. https://doi.org/10.12989/scs.2017.25.1.079.

Shafieifar, M., Farzad, M. and Azizinamini, A. (2017), "Experimental and numerical study on mechanical properties of Ultra High Performance Concrete (UHPC)", *Constr. Build. Mater.*, **156**, 402-411. https://doi.org/10.1016/j.conbuildmat.2017.08.170.

Shim, C.S., Lee, P.G. and Yoon, T.Y. (2004), "Static behavior of large stud shear connectors", *Eng. Struct.*, **26**(12), 1853-1860. https://doi.org/10.1016/j.engstruct.2004.07.011.

Viest, I.M. (1956), "Investigation of stud shear connectors for composite concrete and steel T-beams", *ACI J.*, **27**(8), 875-981.

Wang, J., Qi, J., Teng, T., Xu, Q. and Xiu, H. (2019), "Static behavior of large stud shear connectors in steel-UHPC composite structures", *Eng. Struct.*, **178**, 534-542. https://doi.org/10.1016/j.engstruct.2018.07.058.

Wang, J., Xu, Q., Yao, Y., Qi, J. and Xiu, H. (2018), "Static behavior of grouped large headed stud-UHPC shear connectors in composite structures", *Compos. Struct.*, **206**, 202-214. https://doi.org/10.1016/j.compstruct.2018.08.038.

Wang, J.Y., Gao, X.L. and Yan, J.B. (2018), "Developments and mechanical behaviors of steel fiber reinforced ultra-lightweight cement composite with different densities", *Constr. Build. Mater.*, **171**, 643-653. https://doi.org/10.1016/j.conbuildmat.2018.03.168.

Wang, J.Y., Guo, J.Y., Jia, L.J., Chen, S.M. and Dong, Y. (2017), "Push-out tests of demountable headed stud shear connectors in steel-UHPC composite structures", *Compos. Struct.*, **170**, 69-79. https://doi.org/10.1016/j.compstruct.2017.03.004.

Wang, Z., Nie, X., Fan, J.S., Lu, X.Y. and Ding, R. (2019), "Experimental and numerical investigation of the interfacial properties of non-steam-cured UHPC-steel composite beams", *Constr. Build. Mater.*, **195**, 323-339. https://doi.org/10.1016/j.conbuildmat.2018.11.057.

Xu, X. and Liu, Y. (2016), "Analytical and numerical study of the shear stiffness of rubber-sleeved stud. Journal of Constructional Steel Research", *J. Constr. Steel Res.*, **123**, 68-78. https://doi.org/10.1016/j.jcsr.2016.04.020.

Xue, W.C., Ding, M., Wang, H. and Luo, Z.W. (2008), "Static behavior and theoretical model of stud shear connectors", *J. Bridge Eng.*, **13**(6), 623-634. https://doi.org/10.1061/(ASCE)1084-0702(2008)13:6(623).

CC